Biosensors and Bioelectronics 149 (2020) 111828

Contents lists available at ScienceDirect

Biosensors and Bioelectronics

journal homepage: http://www.elsevier.com/locate/bios

Highly sensitive IRS based biosensor for the determination of cytochrome c as a cancer marker by using nanoporous anodic alumina modified with trypsin

Mahmoud Amouzadeh Tabrizi, Josep Ferré-Borrull, Lluis F. Marsal *

Departamento de Ingeniería Electrónica, Eléctrica y Automática, Universitat Rovira i Virgili, Avda. Països Catalans 26, 43007, Tarragona, Spain

ARTICLE INFO

Keywords:
Cytochrome c
Nanoporous anodic alumina
Interferometric reflectance spectroscopy
Biosensor

ABSTRACT

The determination of cytochrome c in the human serum sample is a regular medical investigation performed to assess cancer diseases. Herein, we used interferometric reflectance spectroscopy (IRS) based biosensor for the determination of cytochrome c. For this purpose first, the nanoporous anodic alumina (NAA) was fabricated. Then, the NAA pore walls were functionalized with 3-aminopropyl trimethoxy silane (NAA-NH_2). Subsequently, the trypsin enzyme was immobilized on the NAA pore walls. The sensing principle of proposed IRS sensor to cytochrome c is based on a change in the intensity of the reflected light to a charge-coupled device (CCD) detector after digesting of cytochrome c by immobilized trypsin enzymes on NAA-NH_2 into the heme-peptide fragment. The heme-peptide fragment then oxidized 2,2'-azino-bis(3-ethylbenzothiazoline-6-sulphonic acid) (ABTS) to green color $ABTS^{\cdot-}$ anion radical in the presence of hydrogen peroxide. The generated green color $ABTS^{\cdot-}$ anion radical solution adsorbed the white light and therefore the intensity of the reflected light from NAA to the CCD decreased. The decrease in the intensity of the white light had a logarithmic relationship with the concentration of the cytochrome c in the range of 1–100 nM. The limit of detections (LOD) for cytochrome c was 0.5 nM. The proposed biosensor exhibited high selectivity, sensitivity, and good stability.

1. Introduction

Signaling molecules are the molecules that are responsible for transmitting information between cells in the body (Manosalva et al., 2015). Cytochrome c (Cyt C) is one of the important signaling molecules of apoptosis or programmed cell death (Hüttemann et al., 2011; Manickam et al., 2017). Cyt C is a potential marker for diagnosing some kinds of cancer diseases, such as lung cancer (Javid et al., 2015), colorectal cancer (Zhang et al., 2016a), and parotid cancer (Giotakis et al., 2010). Since the concentration of Cyt C in human serum is low (~2 nM) (Barczyk et al., 2005; Stepanova et al., 2016), therefore, the fabrication of a highly sensitive sensor to detect it is very important. Up to now, several sensors have been reported for the determination of Cyt C such as electrochemical (Amouzadeh Tabrizi et al., 2017a; Ocaña et al., 2015; Radhakrishnan et al., 2017; Shafaat et al., 2018), and optical (Cai et al., 2019; Liao et al., 2013; Loo et al., 2014; Xia et al., 2012; Yin et al., 2015; Zhang et al. 2019a, 2019b), and mass sensitive piezoelectric (Feifel and Lisdat, 2011) based sensors. Among them, the optical-based sensors are more interested because of the high sensitivity, and contactless ability of them (Loo et al., 2014; Xia et al., 2012). However, the major drawback associated with optical-based sensors such as surface-enhanced Raman scattering (SERS) and surface plasmon resonance (SPR) is the high cost of them. The interferometric reflectance spectroscopy (IRS) is an optical contactless and low-cost sensor that has been used for the determination of the biomolecules (Pol et al., 2019; Ribes et al., 2019; Tabrizi et al., 2019). In this method, the beams of white light interfere with a modified thin film such as nonporous anodic alumina (NAA) and then the partial beams of the light reflected from the thin film to CCD detector. The change in the properties of the light (intensity and wavelength) before and after the interaction of target with this modified thin film can be used as a signal for the quantitative determination of targets. To the best of our knowledge, the use of NAA for the fabrication of the enzymatic sensor based on IRS to detect Cyt C has not been reported yet. To fabricate the sensor, trypsin (Tryp) was immobilized on the pore walls of NAA. Tryp is an enzyme that can cleave the heme proteins to the short peptide chain (Zhang et al., 2016b). The heme group of Cyt C binds to two cysteine residues of the protein through a C–S bond, covalently (Paleus et al., 1955). The peptide fragments of Cyt C containing heme

* Corresponding author.
E-mail address: lluis.marsal@urv.cat (L.F. Marsal).

https://doi.org/10.1016/j.bios.2019.111828
Received 14 June 2019; Received in revised form 10 September 2019; Accepted 28 October 2019
Available online 2 November 2019

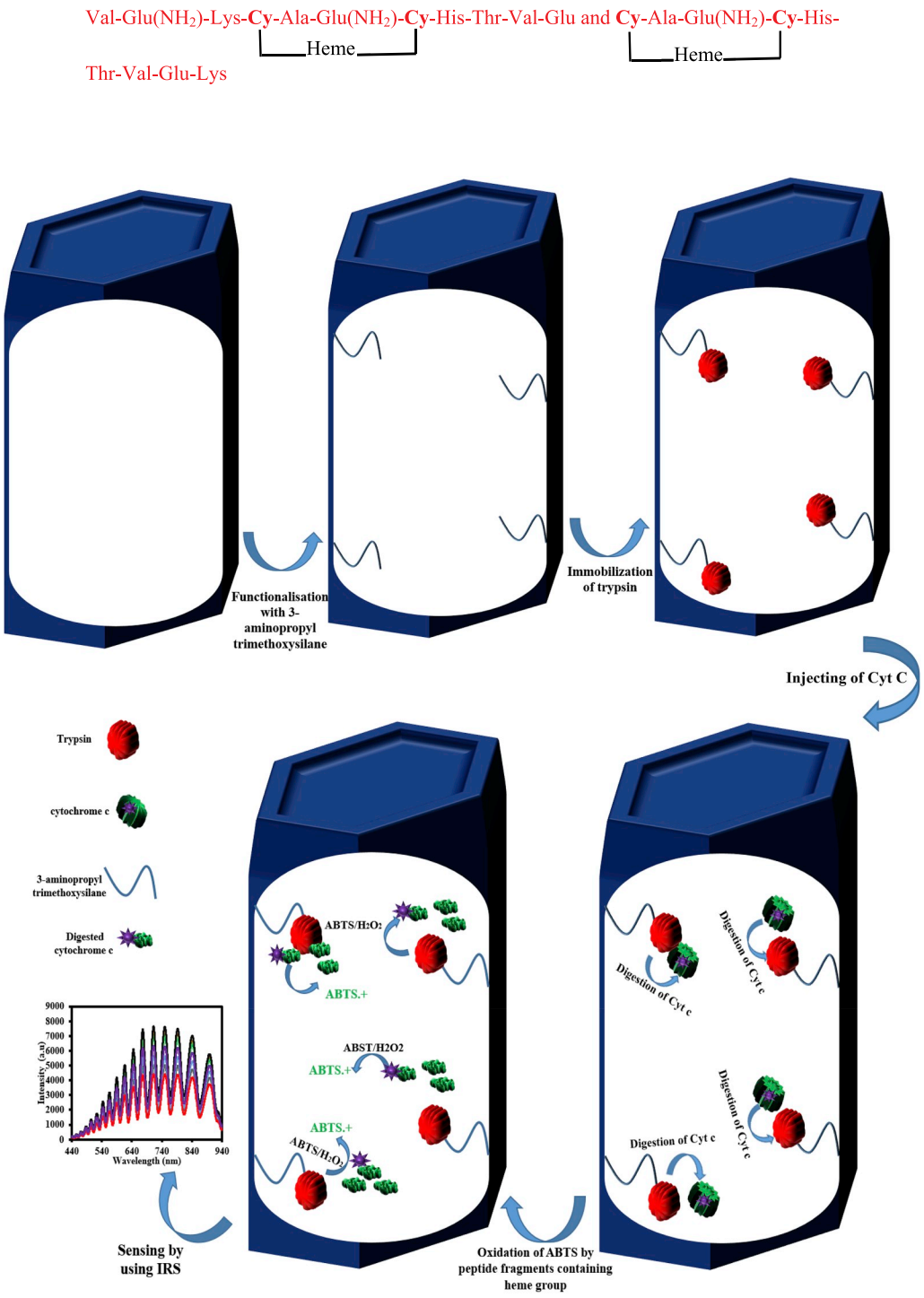

Fig. 1. The schematic illustration for the fabrication of the biosensor.

group are generated by Tryp have these structures:

Theses peptide fragments that bind heme group can oxidase the colorless 2,2'-azino-bis(3-ethylbenzothiazoline-6-sulphonic acid) (ABTS) solution to green collar $ABTS^{\cdot-}$ anion radical solution, in the presence of hydrogen peroxide. The generated green-collar $ABTS^{\cdot-}$ anion radical solution adsorbed the light and therefore, the intensity of the reflected light from NAA modified with Tryp enzyme to the CCD decreased by increasing the concentration of Cyt C. On the basis of these great advantages, the proposed IRS based assay for detecting Cyt C exhibited high analytical performance in terms of sensitivity, stability, selectivity, linear range (LR) and limit of detection (LOD).

2. Experimental section

2.1. Reagents and chemicals

2,2'-azino-bis(3-ethylbenzothiazoline-6-sulfonic acid) (ABTS), 3-aminopropyl trimethoxysilane (3-APES), trypsin (Tryp), cytochrome c (Cyt C), citrate sodium, hydrogen oxide (H_2O_2), phosphoric acid (H_3PO_4), N-hydroxysuccinimide (NHS), 1-Ethyl-3-(3-dimethylamino-propyl) carbodiimide (EDC), chromium (VI) oxide (H_2CrO_4), perchloric acid ($HClO_4$), Human serum albumin (HSA), Human IgG antibody (HIgG), amyloid-beta (AB), and Insulin (IS) were purchased

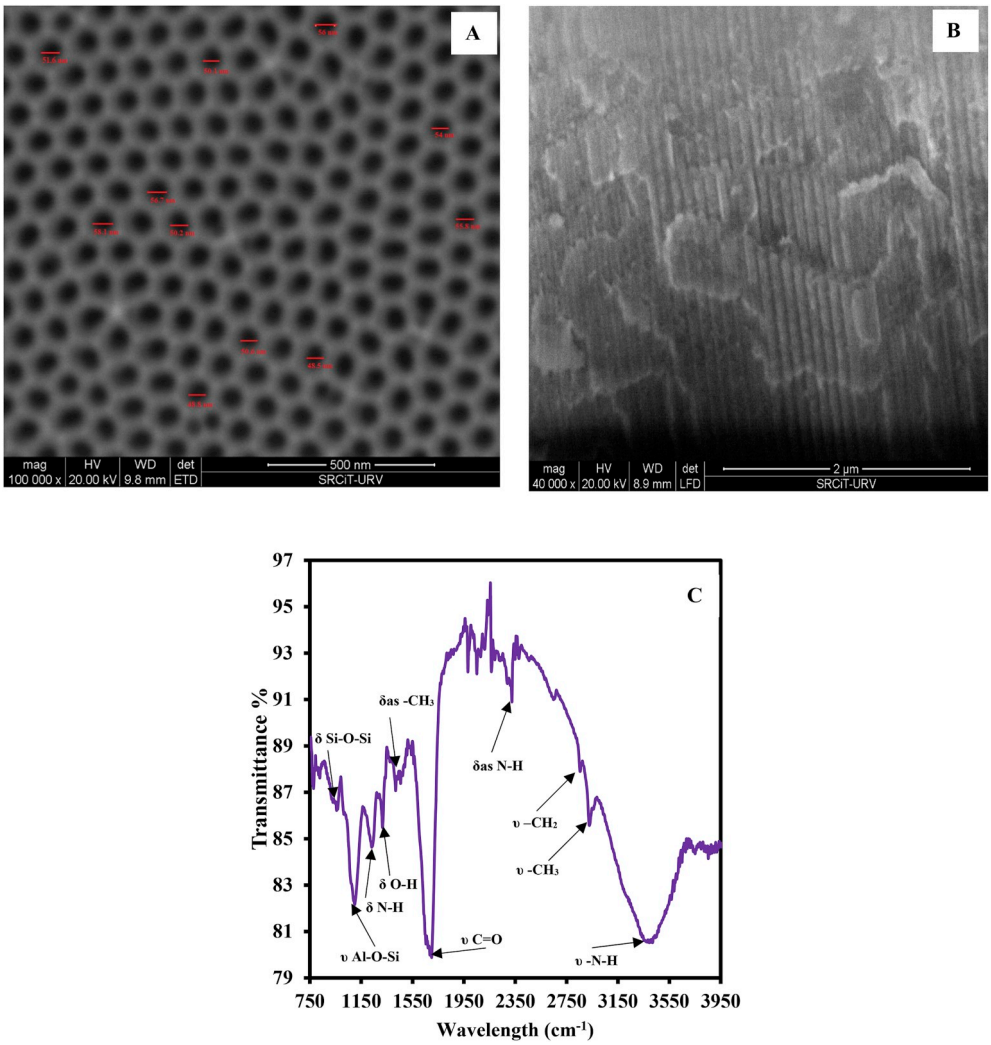

Fig. 2. SEM images of NAA: (A) Top view and (B) cross-section view. (C) FTIR of NAA-NH-GLA-Tryp.

from Sigma-Aldrich. Aluminium (Al) discs of 15 mm diameter were obtained from Goodfellow. Sodium hydroxide (NaOH), and glutaraldehyde (GLA) were obtained from Merck.

2.2. Apparatus

Scanning electron microscopy (SEM) was obtained with an FEI Quanta 600. Fourier transform infrared (FTIR) was performed using a JASCO FT/IR-680Plus spectrometer. The interferometric reflectance spectra were recorded using an AvaSpec-ULS3648 fiber optic spectrometer. UV-visible absorption spectra were recorded using double beams PerkinElmer UV-Vis spectrophotometer.

2.3. Fabrication of NAA-NH_2-Tryp

NAA was prepared and functionalized with 3-APES based on the previous method (Amouzadeh Tabrizi et al., 2019; Santos et al., 2011). The fabrication process is denoted in the electronic supporting material. The fabricated NAA-NH_2 was immersed in a 2.5% GLA in phosphate buffer (PB) and stirred for 1 h. NAA-NH-GLA was then rinsed with water and dried under nitrogen gas flow. NAA-NH-GLA was transferred to Tryp solution (5.0 mL, 100.0 µg mL^{-1}, 0.1 M PB of pH 7.4) and mixed for 6 h at room temperature. During this time, the primary amine group of Tryp enzyme interacted with GLA and immobilized on the substrate covalently. Then, the BSA solution (0.25%, 0.1 M PB of pH 7.4) was dropped on the NAA to decrease the non-specific binding for 30 min. Finally, the substrate was washed with water thoroughly to remove the loosely adsorbed BSA. The fabricated NAA-NH-GLA-Tryp was stored at 4 °C when not in use. The schematic illustration of the NAA-NH-GLA-Tryp fabrication employed is shown in Fig. 1

2.4. The sensing process of Cyt C by using the IRS method

To detect the Cyt C concentration by using the IRS method, the sensor was transferred to a flow cell set-up and the different concentrations of Cyt C solution containing (1.0 mM ABTS and 200.0 µM H_2O_2, pH = 9.4) was pumped by the peristaltic pump to the analytical cell. Under the optimized conditions (pH = 9.4, digestion time: 60 min) at 37 °C, the signal of the sensor was recorded. During the reaction, the immobilized Tryp on NAA digested Cyt C and then the digested Cyt C oxidized the ABTS to green color anion radical $ABTS^{\cdot-}$ in the presence of H_2O_2. Since this green color anion radical can adsorb the wavelength of the light in the range of 400–950 nm (Chen et al., 2017), the intensity of the reflected light to the CCD detector decreased. This decrease in the intensity of the reflected light to the CCD versus the logarithm of the concentration of Cyt C was recorded.

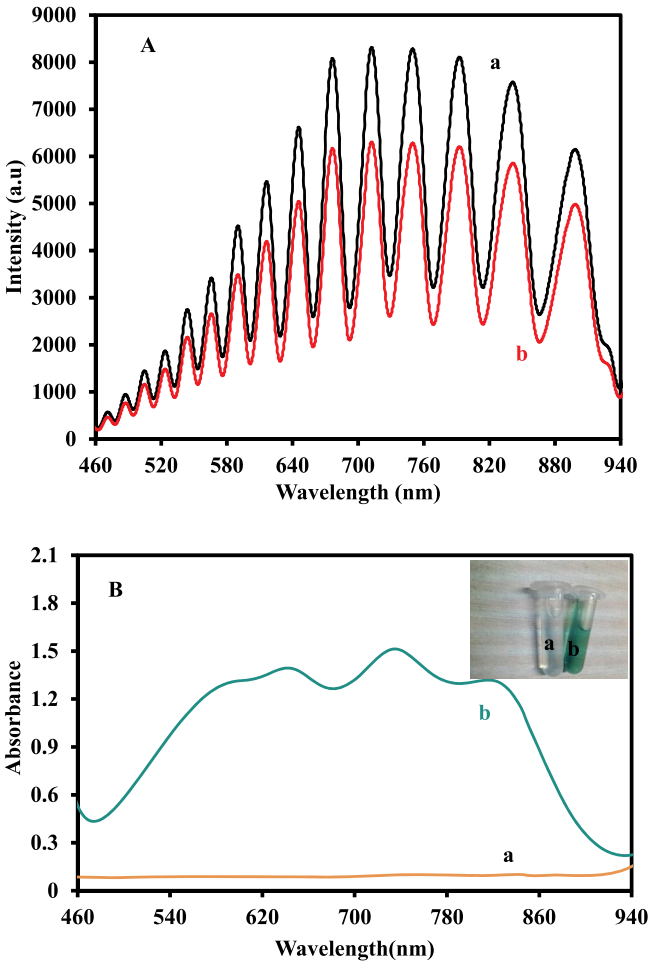

Fig. 3. (A) IRS of the NAA-NH-GLA-Tryp in the measuring solution (1 mM ABTS, 200 μM H_2O_2, pH = 9.4) in the absence (a) and presence of Cyt C (10 nM). (B) Uv-Vis of the measuring solution (1.0 mM ABTS, 200.0 μM H_2O_2, pH 9.4) before (a) and after (b) digesting of Cyt C (10.0 nM) by NAA-NH_2-Tryp.

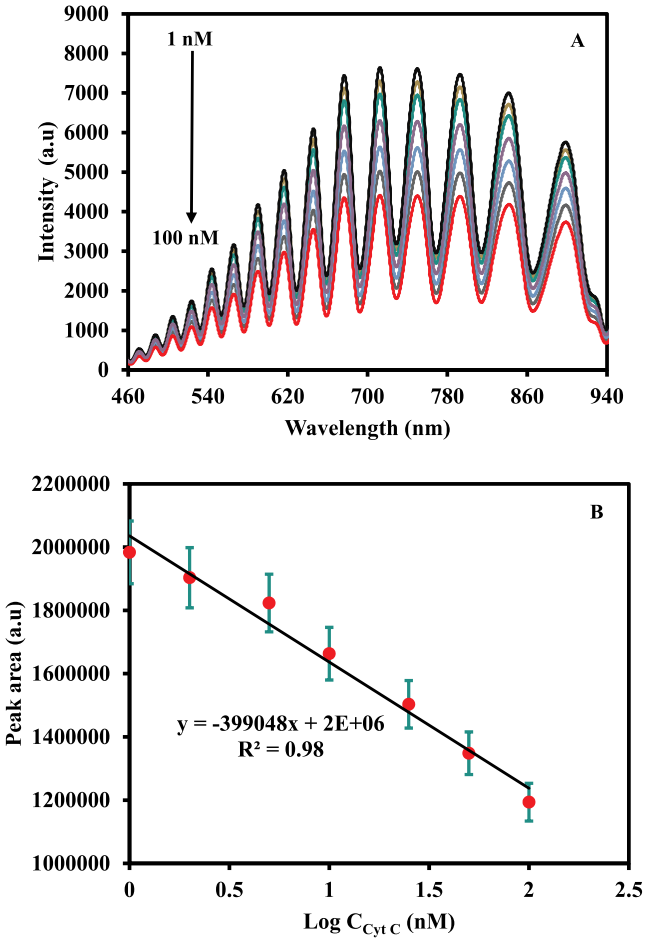

Fig. 4. (A) IRS of the NAA-NH-GLA-Tryp in the measuring solution (1 mM ABTS, 200 μM H_2O_2, pH = 9.4) in the presence of different concentrations of Cyt C (1.0, 2.0, 5.0, 10.0, 25.0, 50.0, and 100.0 nM from outer to inner). (B) The plot of the peak area versus the concentration of Cyt C. Error bars represents standard deviations of five repeated experiments.

3. Results and discussion

3.1. Characterization of nanostructure

Fig. 2A and B shows the top view and (B) cross-section SEM images of NAA, respectively. As can be seen, the NAA has the hexagonal multi-pore structure with an average pore diameter of 53 nm.

Fig. 2C shows a typical FTIR spectrum recorded for NAA-NH-GLA-Tryp in which an absorption band at 3418 cm^{-1} due to N-H bond, a band at 2926 cm^{-1} due to $-CH_3$ stretching, a band at 2890 cm^{-1} due to $-CH_2$ stretching, a band at 2323 cm^{-1} due to –N-H asymmetric stretching, a band at 1698 cm^{-1} due to –C═O vibrating in the amide I structure, a band at 1418 cm^{-1} due to $-CH_3$ asymmetric stretching, a band at 1315 cm^{-1} due to –OH stretching, a band at 1232 cm^{-1} due to the –N-H bending and –C-N stretching, a band at 1100 cm^{-1} due to –Al-O-Si vibrating, and a band at 957 cm^{-1} due to Si-O-Si stretching are also clearly seen (Larkin, 2011). All these results prove that Tryp was immobilized on NAA.

3.2. Optical characterization of sensing interface

Fig. 3A shows the measuring solution (1.0 mM ABTS, 200 μM H2O2, pH 9.4) in the absence (a) and presence of Cyt C (10 nM). As shown, the intensity of the reflected light to the CCD detector in the presence of Cyt C (b) dramatically decreased. The reasonable explanation for this effect is, after the injection of Cyt C to measuring solution, the immobilized Tryp on NAA digested Cyt C to the heme-peptide fragment. The heme-peptide fragment then catalyzed colorless ABTS to green color $ABTS^{\cdot-}$ anion radical. Fig.3B shows the UV-Vis of colorless ABTS (a) and green color $ABTS^{\cdot-}$ anion radical (b) generated by digested Cyt C. As can be seen, the $ABTS^{\cdot-}$ anion radical has a good absorbance in the range 460–940 nm. Therefore, the intensity of the reflected light to the CCD detector after generation of $ABTS^{\cdot-}$ will be decreased. The decrease in the intensity of the reflected light depends on the concentration of Cyt C.

3.3. Optimization of effective parameters on the response of the biosensor

The pH of the solution and digestion time on the response of the biosensor were optimized by using IRS. The Respective figures are given in the electronic supporting material (Fig. S1). The following experimental conditions were found to give the best results: (A) pH of 9.4 the solution, (B) interaction time of 60 min for Cyt C (10.0 nM). As can be seen in Fig. S3A, the immobilized Tryp had the maximum activity to digest Cyt C in solution with a pH of 9.4. The effect of the pH on the activity of Tryp has a good agreement with the previous report (Zhang et al., 2016b).

The effect of digestion time of Tryp on Cyt C was also studied (Fig. S1B). As shown, the response of the IRS based sensor reached to the maximum amount after 60 min and remained unchanged at longer reaction times, suggesting that the cleaved Cyt C oxidized ABTS to its anion radical form adsorbed light by $ABTS^{\cdot-}$ anion radical reached to the

Table 1
Comparison of the analytical performance of the proposed biosensor with other biosensors.

Sensor	Method	LR	LOD	Ref
ITO/Au_{nano}/labeled aptamer	SERS	10–100 nM	2 nM	Xia et al. (2012)
g-C_3N_4-aptamer	Fluorescence	16–140 nM	2.6 nM	(Salehnia et al., 2017)
TGA/CdTe QDs	Fluorescence	0.5–2.5 μM	0.5 μM	Amin et al. (2017)
MIP-coated CdTe QDs composite	Fluorescence	0.97 μM–24 μM	0.41 μM	(Zhang et al., 2011)
DNA/AgNCs	Fluorescence	0–10 μM	14.3 nM	Shamsipur et al. (2016)
UCNP@PDA NP	Fluorescence	0.05–10 μM	20 nM	Ma et al. (2017)
Aptamer/Aunano/Cys/GA/PAMAM/Au electrode	EIS	0.1 nM-10 μM	5.0 nM	Poturnayova et al. (2017)
CcR-CNT-PPy-Pt electrode	CV	1–1000 μM	0.5 μM	Pandiaraj et al. (2013)
Aptameric nanosensor based on βCD-AuNPs	Fluorescence	0.05–10 μM	16.7 nM	Tang et al. (2018)
DNA-AgNCs@tween 80	Fluorescence	0.8 nM–20000 nM	0.8 nM	Qin et al. (2019)
Gold nanoparticle-aptamer/aptamer-peptide-cyanine 5	Fluorescence	20–500 nM	10 nM	Zhang et al. (2017)
N-doped carbon dot (N-doped CD)-based nanosensor	Fluorescence	1–30 μM	0.3 nM	Zhang et al. (2018)
Ag_2S quantum dots	Fluorescence	2–150 nM	1.7 nM	Cai et al. (2019)
NAA-NH-GLA-Tryp	IRS	1–100 nM	0.5 nM	This work

CdSe QDs/GO-CH: CdSe quantum dots with graphene oxide-chitosan; DNA/AgNCs: Aptamer-stabilized silver nanoclusters; CdTe QDs-TGA: Cadmium telluride quantum dots capped with thioglycolic acid; CcR-CNT-PPy-Pt electrode: Cytochrome c reductase carbon nanotubes incorporated polypyrrole/Pt electrode; CV: Cyclic voltammetry; EIS: Electrochemical impedance spectroscopy; UCNP@PDA NP: Up conversion@polydopamine core@shell nanoparticle-based aptameric biosensor.

maximum.

3.4. Determination of Cyt C

Fig. 4A shows the IRS of the proposed method after being exposed to different concentrations of Cyt C. As shown the intensity of the signal decreased by increasing the concentration of Cyt C, therefore the proposed IRS based biosensor for Cyt C sensing is considered as a "signal off" method (Amouzadeh Tabrizi et al., 2017b).

Fig. 4B shows a plot of the signal of IRS, which changes linearly with the logarithm of CytC concentration in the range of 1.0–100.0 nM. The linear regression equation of the calibration curve is expressed as peak area (a.u) = $-399048 \log (C_{Cyt\ C})$ (nM) $+2 \times 10^6$ with a correlation coefficient of 0.98. The limit of detection (LOD) is 0.5 nM (based as 3σ/S, where σ is the standard deviation of the blank and S is the slope of the calibration curve).

The comparison of the analytical performance of the proposed assay is summarized in Table 1. It can be seen that the analytical performance of the proposed assay methods is comparable with other biosensors and the proposed IRS method has a good sensitivity to detect Cyt C cancer marker. As it is obvious from Table 1, the proposed enzyme-based IRS sensor not only is a remote biosensor but also is a cheap and high sensitive biosensor for the assay of Cyt C, in comparison with SERS-based (Xia et al., 2012) and fluorescence-based assay (Qin et al., 2019).

3.5. The influence of interference, reproducibility, stability, and the practical application of the proposed IRS sensor

The effect interfering compounds were also studied on the assay of Cyt C cancer marker by using the IRS method (Fig. S2). No sensible interference was observed with urea, glucose, dopamine, HIgG, HSA, IS, and AB for 10-fold quantities of Cyt C (10.0 nM). As it can be clearly seen that the proposed Cyt C assay has high selectivity. To investigate the stability of NAA-NH-GLA-Tryp, it was stored at 4 °C for 14 days immersed in a PB of pH 7.4. The IRS intensity decreased only by 7.3%. This high stability of the assay method can be related to the biocompatibility of NAA keep activities of the immobilized biomaterials (La Flamme et al., 2007; Santos et al., 2012). The reproducibility was also evaluated for determinations of 10.0 nM of Cyt C with five different NAA-NH-GLA-Tryp. The relative standard deviation (RSD) was 5.2% for Cyt C.

To investigate the practical application of the proposed biosensor, NAA-NH-GLA-Tryp was employed for the determination of Cyt C in human serum. Briefly, the human serum sample was first diluted 10.0 times with PB solution (0.1 M, pH 9.4). Then, 1.8 mL of the diluted human serum sample was mixed with 0.2 mL Cyt C (250 nM) and pumped into the cell to be analysed. The recovery of the analysis was 97.6% by using a standard addition method (Table S1). The result proves that the NAA-NH-GLA-Tryp had excellent analytical performance for Cyt C.

4. Conclusions

This study introduced two novel assay methods based on the IRS for the determination of Cyt C. To fabricate sensor, the Tryp enzyme was immobilized on an amino-silanized NAA via GLA cross linker. During the measuring process, the immobilized Tryp enzyme digested the Cyt C to the heme-peptide fragment, letting an intensive catalytic role on ABTS oxidization in the presence of H2O2. In comparison with ABTS solution that is colorless, the generated green color $ABTS^{\cdot-}$ anion radical solution can absorb the light. Therefore the intensity of the reflected light to the CCD detector decreased by increasing Cyt C concentration. The IRS based biosensor signals had a logarithmic relationship with the concentration of Cyt C. Despite these characteristics, there is a major limitation of the assay method. This assay method cannot be used for the fabrication of the wearable sensor.

Declaration of competing interest

The authors declare that they have no known competing financial interests or personal relationships that could have appeared to influence the work reported in this paper.

CRediT authorship contribution statement

Mahmoud Amouzadeh Tabrizi: Conceptualization, Methodology, Data curation, Formal analysis, Validation, Investigation, Visualization, Writing - original draft. **Josep Ferré-Borrull:** Formal analysis, Validation. **Lluis F. Marsal:** Conceptualization, Supervision, Writing - review & editing, Resources, Project administration, Funding acquisition.

Acknowledgments

This research was partially supported by the Spanish Ministerio de Ciencia, Innovación y Universidades (MICINN/FERDER) RTI2018-094040-B-I00, by the Agency for Management of University and Research Grants (AGAUR) ref. 2017-SGR-1527, by the Catalan Institution for Research and Advanced Studies under the ICREA Academia Award and by the University Rovira i Virgili, Martí-Franquès II post-doctoral program under grant number 2017PMF-POST2-7. The project

leading to these results has also received funding from "la Caixa" foundation under the agreement LCF/PR/PR17/11120023.

Appendix A. Supplementary data

Supplementary data to this article can be found online at https://doi.org/10.1016/j.bios.2019.111828.

References

Amin, R.M., Elfeky, S.A., Verwanger, T., Krammer, B., 2017. Biosens. Bioelectron. 98, 415–420.

Amouzadeh Tabrizi, M., Ferré-Borrull, J., Marsal, L.F., 2019. Biosens. Bioelectron. 137, 279–286.

Amouzadeh Tabrizi, M., Shamsipur, M., Saber, R., Sarkar, S., 2017. Sens. Actuators B Chem. 240, 1174–1181.

Amouzadeh Tabrizi, M., Shamsipur, M., Saber, R., Sarkar, S., Besharati, M., 2017. Microchim. Acta 185, 59–65.

Barczyk, K., Kreuter, M., Pryjma, J., Booy, E.P., Maddika, S., Ghavami, S., Berdel, W.E., Roth, J., Los, M., 2005. Int. J. Cancer 116, 167–173.

Cai, M., Ding, C., Cao, X., Wang, F., Zhang, C., Xian, Y., 2019. Anal. Chim. Acta 1056, 153–160.

Chen, Q., Liang, C., Sun, X., Chen, J., Yang, Z., Zhao, H., Feng, L., Liu, Z., 2017. Proc. Natl. Acad. Sci. U.S.A. 114, 5343–5348.

Feifel, S.C., Lisdat, F., 2011. J. Nanobiotechnol. 9, 59-59.

Giotakis, J., Gomatos, I.P., Alevizos, L., Georgiou, A.N., Leandros, E., Konstadoulakis, M. M., Manolopoulos, L., 2010. Otolaryngol. Head Neck Surg. 142, 605–611.

Hüttemann, M., Pecina, P., Rainbolt, M., Sanderson, T.H., Kagan, V.E., Samavati, L., Doan, J.W., Lee, I., 2011. Mitochondrion 11, 369–381.

Javid, J., Mir, R., Julka, P.K., Ray, P.C., Saxena, A., 2015. Tumor Biol. 36, 4253–4260.

La Flamme, K.E., Popat, K.C., Leoni, L., Markiewicz, E., La Tempa, T.J., Roman, B.B., Grimes, C.A., Desai, T.A., 2007. Biomaterials 28, 2638–2645.

Larkin, P., 2011. Chapter 6 - IR and Raman spectra-structure correlations: characteristic group frequencies. In: Larkin, P. (Ed.), Infrared and Raman Spectroscopy. Elsevier, Oxford, pp. 73–115.

Liao, D., Chen, J., Li, W., Zhang, Q., Wang, F., Li, Y., Yu, C., 2013. Chem. Commun. 49, 9458–9460.

Loo, F.-C., Ng, S.-P., Wu, C.-M.L., Kong, S.K., 2014. Sens. Actuators B Chem. 198, 416–423.

Ma, L., Liu, F., Lei, Z., Wang, Z., 2017. Biosens. Bioelectron. 87, 638–645.

Manickam, P., Kaushik, A., Karunakaran, C., Bhansali, S., 2017. Biosens. Bioelectron. 87, 654–668.

Manosalva, P., Manohar, M., von Reuss, S.H., Chen, S., Koch, A., Kaplan, F., Choe, A., Micikas, R.J., Wang, X., Kogel, K.-H., Sternberg, P.W., Williamson, V.M., Schroeder, F.C., Klessig, D.F., 2015. Nat. Commun. 6, 7795–7803.

Ocaña, C., Lukic, S., del Valle, M., 2015. Microchim. Acta 182, 2045–2053.

Paleus, S., Ehrenberg, A., Tuppy, H., 1955. Acta Chem. Scand. 9, 365–374.

Pandiaraj, M., Madasamy, T., Gollavilli, P.N., Balamurugan, M., Kotamraju, S., Rao, V.K., Bhargava, K., Karunakaran, C., 2013. Bioelectrochemistry 91, 1–7.

Pol, L., Eckstein, C., Acosta, L.K., Xifré-Pérez, E., Ferré-Borrull, J., Marsal, L.F., 2019. J. Nanomater. 9, 478–490.

Poturnayova, A., Castillo, G., Subjakova, V., Tatarko, M., Snejdarkova, M., Hianik, T., 2017. Sens. Actuators B Chem. 238, 817–827.

Qin, Y., Daniyal, M., Wang, W., Jian, Y., Yang, W., Qiu, Y., Tong, C., Wang, W., Liu, B., 2019. Sens. Actuators B Chem. 291, 485–492.

Radhakrishnan, J., Origenes, R., Littlejohn, G., Nikolich, S., Choi, E., Smite, S., Lamoureux, L., Baetiong, A., Shah, M., Gazmuri, R.J., 2017. Biomark. Insights 12, 1–10.

Ribes, A., Aznar, E., Santiago-Felipe, S., Xifré-Pérez, E., Tormo-Mas, M.Á., Peman, J., Marsal, L.F., Martinez-Manez, R., 2019. ACS Sens. 4, 1291–1298.

Salehnia, F., Hosseini, M., Ganjali, M.R., 2017. Microchim. Acta 184, 2157–2163.

Santos, A., Formentín, P., Pallarès, J., Ferré-Borrull, J., Marsal, L.F., 2011. J. Electroanal. Chem. 655, 73–78.

Santos, A., Macías, G., Ferré-Borrull, J., Pallarès, J., Marsal, L.F., 2012. ACS Appl. Mater. Interfaces 4, 3584–3588.

Shafaat, A., Faridbod, F., Ganjali, M.R., 2018. New J. Chem. 42, 6034–6039.

Shamsipur, M., Molaabasi, F., Hosseinkhani, S., Rahmati, F., 2016. Anal. Chem. 88, 2188–2197.

Stepanova, V.B., Shurpik, D.N., Evtugyn, V.G., Stoikov, I.I., Evtugyn, G.A., Osin, Y.N., Hianik, T., 2016. Sens. Actuators B Chem. 225, 57–65.

Tabrizi, M.A., Ferré-Borrull, J., Marsal, L.F., 2019. Biosens. Bioelectron. 137, 279–286.

Tang, J., Huang, C., Shu, J., Zheng, J., Ma, D., Li, J., Yang, R., 2018. Anal. Chem. 90, 5865–5872.

Xia, Y., Gao, P., Qiu, X., Xu, Q., Gan, S., Yang, H., Huang, S., 2012. Analyst 137, 5705–5709.

Yin, X., Cai, J., Feng, H., Wu, Z., Zou, J., Cai, Q., 2015. New J. Chem. 39, 1892–1898.

Zhang, H., Kou, Y., Li, J., Chen, L., Mao, Z., Han, X.X., Zhao, B., Ozaki, Y., 2019. Anal. Chem. 91, 1213–1216.

Zhang, H., Zhang, B., Di, C., Ali, M.C., Chen, J., Li, Z., Si, J., Zhang, H., Qiu, H., 2018. Nanoscale 10, 5342–5349.

Zhang, J., Ma, X., Wang, Z., 2019. Anal. Chem. 91, 6600–6607.

Zhang, K., Chen, Y., Huang, X., Qu, P., Pan, Q., Lü, L., Jiang, S., Ren, T., Su, H., 2016. Arch. Med. Sci. 12, 68–77.

Zhang, L., Qin, H., Cui, W., Zhou, Y., Du, J., 2016. Talanta 161, 535–540.

Zhang, W., He, X.-W., Chen, Y., Li, W.-Y., Zhang, Y.-K., 2011. Biosens. Bioelectron. 26, 2553–2558.

Zhang, X., Liao, N., Chen, G., Zheng, A., Zeng, Y., Liu, X., Liu, J., 2017. Nanoscale 9, 10861–10868.